Atmos. Chem. Phys., 18, 5847–5860, 2018
https://doi.org/10.5194/acp-18-5847-2018

Atmospheric Chemistry and Physics
Open Access
EGU

Study of the daily and seasonal atmospheric CH_4 mixing ratio variability in a rural Spanish region using ^{222}Rn tracer

Claudia Grossi[1,a,b], **Felix R. Vogel**[2], **Roger Curcoll**[1,c], **Alba Àgueda**[1,d], **Arturo Vargas**[3], **Xavier Rodó**[1,4,e], **and Josep-Anton Morguí**[1,5,c]

[1]Institut Català de Ciències del Clima (IC3), Barcelona, Spain
[2]Climate Research Division, Environment and Climate Change Canada, Toronto, Canada
[3]Institut de Tècniques Energètiques (INTE), Universitat Politècnica de Catalunya (UPC), Barcelona, Spain
[4]Institució Catalana de Recerca i Estudis Avançats (ICREA), Barcelona, Spain
[5]Departament Biologia Evolutiva, Ecologia i Ciències Ambientals, Universitat de Barcelona (UB), Barcelona, Spain
[a]present address: Institut de Tècniques Energètiques (INTE), Universitat Politècnica de Catalunya (UPC), Barcelona, Spain
[b]present address: Physics Department, Universitat Politècnica de Catalunya (UPC), Barcelona, Spain
[c]present address: Institut de Ciència i Tecnologia Ambientals (ICTA), Universitat Autònoma de Barcelona (UAB), Cerdanyola del Vallès, Spain
[d]present address: Centre d'Estudis del Risc Tecnològic, Universitat Politècnica de Catalunya (UPC) – BarcelonaTech, Barcelona, Spain
[e]present address: CLIMA2, Climate and Health Program, ISGlobal (Barcelona Institute of Global Health), Barcelona, Spain

Correspondence: Claudia Grossi (claudia.grossi@upc.edu) and Felix R. Vogel (felix.vogel@canada.ca)

Received: 19 May 2017 – Discussion started: 6 October 2017
Revised: 26 March 2018 – Accepted: 6 April 2018 – Published: 26 April 2018

Abstract. The ClimaDat station at Gredos (GIC3) has been continuously measuring atmospheric (dry air) mixing ratios of carbon dioxide (CO_2) and methane (CH_4), as well as meteorological parameters, since November 2012. In this study we investigate the atmospheric variability of CH_4 mixing ratios between 2013 and 2015 at GIC3 with the help of co-located observations of ^{222}Rn concentrations, modelled ^{222}Rn fluxes and modelled planetary boundary layer heights (PBLHs). Both daily and seasonal changes in atmospheric CH_4 can be better understood with the help of atmospheric concentrations of ^{222}Rn (and the corresponding fluxes). On a daily timescale, the variation in the PBLH is the main driver for ^{222}Rn and CH_4 variability while, on monthly timescales, their atmospheric variability seems to depend on emission changes. To understand (changing) CH_4 emissions, nocturnal fluxes of CH_4 were estimated using two methods: the radon tracer method (RTM) and a method based on the EDGARv4.2 bottom-up emission inventory, both using FLEXPARTv9.0.2 footprints. The mean value of RTM-based methane fluxes (FR_CH_4) is 0.11 mg CH_4 m^{-2} h^{-1} with a standard deviation of 0.09 or 0.29 mg CH_4 m^{-2} h^{-1} with a standard deviation of 0.23 mg CH_4 m^{-2} h^{-1} when using a rescaled ^{222}Rn map (FR_CH_4_rescale). For our observational period, the mean value of methane fluxes based on the bottom-up inventory (FE_CH_4) is 0.33 mg CH_4 m^{-2} h^{-1} with a standard deviation of 0.08 mg CH_4 m^{-2} h^{-1}. Monthly CH_4 fluxes based on RTM (both FR_CH_4 and FR_CH_4_rescale) show a seasonality which is not observed for monthly FE_CH_4 fluxes. During January–May, RTM-based CH_4 fluxes present mean values 25 % lower than during June–December. This seasonal increase in methane fluxes calculated by RTM for the GIC3 area appears to coincide with the arrival of transhumant livestock at GIC3 in the second half of the year.

1 Introduction

The impact of the atmospheric increase in greenhouse gases (GHGs) on climate change is well known (IPCC, 2013). GHG emissions, due to natural as well as anthropogenic sources, are currently estimated and reported by each na-

tional agency to the United Nations Framework Convention on Climate Change (UNFCCC). A better understanding of the underlying processes causing these emissions can help in the implementation of future emission reduction strategies. Methane (CH_4) is the second most important anthropogenic GHG that is covered by the UNFCCC. The atmospheric mixing ratio of CH_4 has substantially changed since pre-industrial times from a global average of 715 nmol mol^{-1} to more than 1774 nmol mol^{-1} (IPCC, 2013). Nowadays, the contribution of CH_4 related to anthropogenic activities in the atmosphere represents about 25 % of total additional anthropogenic radiative forcing (IPCC, 2013). However, CH_4 has a relatively short lifetime in the atmosphere ($\sim$ 9 years) and this makes it relevant in defining immediate and efficient emission reduction strategies (Prinn et al., 2000). Particularly in Spain, man-made methane emissions are mainly due to enteric fermentation (38 %), management of manure (20 %) and landfills (36 %) (WWF, 2014; MMA, 2016). The remaining methane contributions in Spain are due to rice cultivation (e.g. Àgueda et al., 2018), coal mining, leaks in natural gas infrastructures and waste water treatment. The CH_4 emission due to enteric fermentation related to livestock is directly linked to the number of animals of each type or breed of cattle, their age, their diet and environmental conditions (MMA, 2016). Spanish CH_4 emissions due to enteric fermentation were estimated to be 11 704 Gg CO_2^{-eq} (MMA, 2016).

In order to estimate GHG emissions, bottom-up (based on fuel consumption and anthropogenic activity data) and top-down methods (based on atmospheric observations and modelling) are both widely applied and the scientific community has focussed on reducing their related uncertainties and understanding systematic inconsistencies (e.g. Vermeulen et al., 2006; Bergamaschi et al., 2010; NRC, 2010; Jeong et al., 2013; Hiller et al., 2014). Top-down methods usually require both high-quality and long-term GHG observations. European projects, such as InGOS (www.ingos-infrastructure.eu, last access: March 2018), and infrastructures, such as ICOS (www.icos-infrastructure.eu, last access: April 2018), aim to offer atmospheric CO_2 and non-CO_2 GHG data and data products to better understand GHG fluxes in Europe and adjacent regions.

Unfortunately, in some European regions, such as Spain, there is still a significant lack of high-quality atmospheric GHG observations. The Catalan Institute of Climate Sciences (IC3) has been working since 2010 within the ClimaDat project in setting up a network of stations in national parks for continuous measurements of mixing ratios of GHGs, tracers and meteorological parameters (www.climadat.es, last access: April 2018). The IC3 network mainly aims to monitor and study the exchange of GHGs between the land surface and the lower atmosphere (troposphere) in different ecosystems, which are characterized by different biogenic and anthropogenic processes, under different synoptic conditions.

Besides GHG mixing ratios, co-located observations of additional gases can provide us with useful tracers for source apportionment studies or to help us to better understand atmospheric processes (e.g. Zahorowski et al., 2004). The radioactive noble gas radon (^{222}Rn), due to its chemical and physical characteristics (e.g. Nazaroff and Nero, 1988), is being extensively used for studying atmosphere dynamics, such as boundary layer evolution (e.g. Galmarini, 2006; Vinuesa and Galmarini, 2007), and soil–atmosphere exchanges (e.g. Schery et al., 1998; Zahorowski et al., 2004; Szegvary et al., 2009; Grossi et al., 2012, 2016; Vargas et al., 2015). European GHG-monitoring infrastructures already include atmospheric ^{222}Rn monitors in their stations (e.g. Arnold et al., 2010; Zimnoch et al., 2014; Schmithüsen et al., 2017). The co-evolution of atmospheric ^{222}Rn and GHG concentrations can also be used within the radon tracer method (RTM) to estimate local and regional GHG fluxes (e.g. Van der Laan et al., 2010; Levin et al., 2011; Vogel et al., 2012; Wada et al., 2013; Grossi et al., 2014).

In this study we analysed the time series of atmospheric CH_4 mixing ratios measured at the IC3 station in Gredos and Iruelas (GIC3) between January 2013 and December 2015. The main aim was to investigate the main drivers that influence the daily and seasonal variability of methane concentrations in this mountainous rural southern European region. The GIC3 station is located on the Spanish plateau, an area mainly characterized by livestock activity and where transhumance is still practiced (Ruiz Perez and Valero Sáez, 1990). This is an ancestral activity consisting of the seasonal movement of livestock over long distances to reach warmer regions during the winter together with a return to the mountains in summer where pastures are greener and more suitable for grazing activities (Ruiz Perez and Valero Sáez, 1990; López Sáez et al., 2009). The livestock leaves the GIC3 region to go to southern Spanish regions during the cold period. The enteric fermentation due to digestive processes in animals could thus be a significant CH_4 source in this area. The Unión de Pequeños Agricultores (UPA, 2009) reports that between 2004 and 2009 an average of 800 000 transhumant animals were hosted in Spain and 40 000 (5 % of total) were counted in the province of Ávila (extension: 8048 km^2), where the GIC3 station is located. According to the available literature, in this area 85 % of livestock still performs transhumance, with 500 stockbreeders moving every winter from the Gredos national park (GNP) to warmer areas of Spain, such as Extremadura (Ruiz Perez and Valero Sáez, 1990; López Sáez et al., 2009; Libro Blanco, 2013). Generally, this mobility of cattle and associated CH_4 emissions (i.e. a major regional CH_4 source) cannot easily be included in country-wide (annual) inventories because it has not yet been properly quantified and reported by nations. The present study aims to highlight the utility of ^{222}Rn as a tracer to retrieve independent GHG fluxes on a monthly basis using atmospheric ^{222}Rn and CH_4 data. This work represents a first step towards a better characterisation of transient sources, such as transhumant livestock for CH_4, which could help to improve national emissions inventories. Finally, it offers new

CH_4 data for an under-sampled area which will help in the improvement of the regional and global methane budgets.

GIC3 is a new atmospheric station so its location, the surrounding region and the instrumentation used at this station are described in the methodology section of this paper. In the first part of the results section both the daily and seasonal changes in CH_4 mixing ratios observed at the GIC3 station have been analysed in relation to ^{222}Rn and PBLH variability. In the second part, the nocturnal CH_4 fluxes and their monthly variability have been estimated by the RTM, following Vogel et al. (2012), and using an emission inventory for CH_4 (EDGARv4.2). Both flux estimation methods have been applied using the same source region as modelled by the atmospheric transport model FLEXPARTv9.0.2. The possible influence of large cities surrounding GIC3 and of seasonally changing meteorological conditions on the retrieved CH_4 fluxes has also been investigated. Finally, the difference in CH_4 fluxes between the cattle season, when livestock is present in the GIC3 region, and the no-cattle season, when the transhumant cattle have migrated to the south of Spain, calculated using the RTM, has been estimated.

2 Methods

2.1 Study site: Gredos and Iruelas station (GIC3)

The Gredos and Iruelas station is located in a rural region of the Spanish central plateau (40.35° N, 5.17° E; 1440 m above sea level – a.s.l.), as shown in Fig. S1 of the Supplement. GIC3 is located on the west side of the GNP, which has a total extension of 86 397 ha. The mountains of the GNP form the highest mountain range in the east–west-orientated central mountain system. The GNP has a, predominantly, granitic basement and is thus covered by soil with high activity levels of ^{228}U (Nazaroff and Nero, 1988). The average ^{222}Rn flux in this area is about 70–100 Bq m^{-2} h^{-1} (e.g. López-Coto et al., 2013; Karstens et al., 2015), which is almost twice the average radon flux in central Europe (Szegvary et al., 2009, López-Coto et al., 2013; Grossi et al., 2016). The vegetation in the GIC3 area is stratified according to altitude and the main land use practice is a mixture of agro-forestry exploitation (EEA, 2013)

Livestock farming is one of the main economic activities in the area around the GIC3 station (Ruiz Perez and Valero Sáez, 1990; López Saéz et al., 2009; MMA, 2016; Hernández, 2016). In the GNP the seasonal migration of livestock starts between November and December, when they travel to the south of the Iberian Peninsula, and they do not return until late May–mid-June (Ruiz Perez and Valero Sáez, 1990). In Fig. S2, a map of the main Spanish transhumant paths is presented. Unfortunately, no specific reports of cattle mobility data are so far available for the GIC3 area.

Besides livestock activities, there are three small-sized to medium-sized water reservoirs and four medium-sized to large cities in the wider area surrounding GIC3. The water reservoirs as well as several facilities present in the cities, e.g. landfills or waste water treatment plants, represent CH_4 sources which could also influence methane concentrations observed at the GIC3 station under specific synoptic conditions. The water reservoirs are located in the west and north-west area of GIC3: (i) The Gabriel and Galan reservoir with an extension of 4683 ha (40.25° N; −6.13° E; 80 km away from GIC3), (ii) Santa Teresa with an extension of 2663 ha (40.60° N; −5.58° E; 42 km away from GIC3), and (iii) Almendra with an extension of 7940 ha (41.25° N; −6.26° E; 120 km away from GIC3). The metropolitan area of Madrid, which comprises about 6.3 million inhabitants, is situated approximately 120 km to the east of GIC3. Valladolid, located 150 km to the west of GIC3, is reported to have approximately 416 000 inhabitants, while smaller cities like Salamanca (84 km to the north-west) and Ávila (55 km to the north-east) only have 229 000 and 59 000 inhabitants, respectively. More information about these four cities is reported in Table S1 of the Supplement.

2.2 Atmospheric measurements of CH_4 and ^{222}Rn

2.2.1 Air sampling

Atmospheric CH_4, CO_2 and ^{222}Rn concentrations have been continuously measured since November 2012 at the GIC3 station (air inlet 20 m above ground level (a.g.l.) tower). CH_4 and CO_2 are measured with a frequency of 0.2 Hz using a G2301 analyser (Picarro Inc., USA). Hourly atmospheric ^{222}Rn concentrations are measured using an atmospheric radon monitor (ARMON) (Grossi et al., 2012, 2016). A schematic diagram of the measurement set-up used at the GIC3 station is shown in Fig. S3.

The Picarro Inc. G2301 analyser is calibrated every 2 weeks using four secondary working gas standards, which are calibrated at the beginning and end of their lifetime against seven standards of the National Oceanic and Atmospheric Administration (NOAA) (calibration scales are WMO-CO_2-X2007 and WMO-CH_4-X2004 for CO_2 and CH_4, respectively). A target gas is analysed daily for 20 min in order to check the stability and quality of the instrument calibration. For the length of the study, the instrument repeatability for CH_4 was 0.80 nmol mol^{-1}, the long-term reproducibility was 0.36 nmol mol^{-1} and the observe bias was 0.81 nmol mol^{-1}. Previous values were calculated according to the definitions of the World Meteorological Organization (WMO, 2009). The ARMON instrument was installed at the GIC3 station in collaboration with the Institute of Energetic Techniques of the Universitat Politècnica de Catalunya (INTE-UPC). The ARMON is a self-designed instrument based on α spectrometry of ^{218}Po, collected electrostatically on a passive implanted detector. The monitor has a minimum

detectable activity of 150 mBq m^{-3} (Grossi et al., 2012). The performance of the ARMON was previously tested against a widely used ^{222}Rn progeny monitor and good results were observed (Grossi et al., 2016).

The responses of both the ARMON and G2301 analysers are influenced by the air sample humidity level. Water correction factors for both instruments are empirically determined and corrected following Grossi et al. (2012) and Rella (2010), respectively.

2.2.2 Sample air drying system

The instruments used at the GIC3 station require a total flow of 2.5 L min^{-1} of sample air dried to a water concentration lower than 1000 ppm to perform simultaneous measurements of GHG and ^{222}Rn concentrations. In the GIC3 inlet system, as shown in Fig. S3, the sample air is passed through a Nafion® membrane (Permapure, PD-100T-24MPS) that exchanges water molecules with a dry counter-current air flow. The counter-current air flow is dried in a two-step process, first through a cooling coil in a refrigerator at 3 °C and a pressure of 5.5 barg, and then a cryotrap is used at −70 °C and a pressure of 1.5 barg. Multiple cryotraps are selected with electrovalves in order to increase the autonomy of the system to about 2 months. The typical water content of sample air inside the instruments is between 100 and 200 ppm.

2.2.3 Meteorological observations

Meteorological variables are continuously measured at the GIC3 tower. The canopy around the tower is below 20 m. The area surrounding the GIC3 station is hilly as shown on the topographic map of Fig. S1. The tower is equipped with (1) two-dimensional sonic anemometer (WindSonic, Gill Instruments) for wind speed and direction (accuracies of ±2 % and ±3°, respectively); (2) humidity and temperature probe (HMP 110, Vaisala) with an accuracy of ±1.7 % and ±0.2 °C, respectively; (3) barometric pressure sensor (61302V, Young Company) with an accuracy of 0.2 hPa (at 25 °C) and 0.3 hPa (from −40 to +60 °C). All the accuracies refer to the manufacturer's specifications.

2.3 Planetary boundary layer height (PBLH)

Planetary boundary layer height (PBLH) data used in this analysis have been extracted from the operational high-resolution atmospheric model of the European Centre for Medium-Range Weather Forecasting (ECMWF-HRES) (ECMWF, 2006) for the period of interest (January 2013–December 2015) for the GIC3 area. This model stores output variables every 12 h (at 00:00 and 12:00 UTC) with a temporal resolution output of 1 h and with forecasts from +00:00 to +11:00 h. The horizontal spatial resolution of the model is about 16 km. In the ECMWF-HRES model the calculation of the PBLH is based on the bulk Richardson number (Ri) (Troen and Mahrt, 1986). As regards the reliability of modelled PBLH data, Seidel et al. (2012) have shown that data limitations in vertical profiles introduce height uncertainties that can exceed 50 % for shallow boundary layers (< 1 km), but are generally < 20 % for deeper boundary layers. In addition, they compared radiosonde observations with re-analysis and climate models and showed that these latter two produce deeper layers due to the difficulty in simulating stable conditions.

2.4 CH_4 fluxes

2.4.1 CH_4 fluxes based on FLEXPART footprints and the radon tracer method

The RTM is a well-known method (e.g. Hammer and Levin, 2009) and it has been used in this study, following Vogel et al. (2012), in order to obtain observation-based estimates of nocturnal CH_4 fluxes at GIC3. The RTM uses atmospheric measurements of ^{222}Rn and measured, or modelled, values of ^{222}Rn fluxes together with atmospheric mixing ratios of a gas of interest, i.e. CH_4, in order to retrieve the net fluxes of this gas (e.g. Hammer and Levin, 2009; Grossi et al., 2014). This method is based on the assumption that the nocturnal lower atmospheric boundary layer can be described as a well-mixed box of air (Schmidt et al., 1996; Levin et al., 2011; Vogel et al., 2012). The boundary layer is considered homogeneous within the box and with a time-varying height. No significant horizontal advection is considered due to stable atmospheric conditions (Griffiths et al., 2012). In this atmospheric volume the variation of the concentration of any tracer (shown with the subindex i) with time $C_i(t)$ will be proportional to the flux of the tracer $F_i(t)$ and inversely proportional to the height of the boundary layer $h(t)$ (Eq. 1; e.g. Galmarini, 2006; Griffiths et al., 2012; Vogel et al., 2012; Grossi et al., 2014).

$$\frac{\mathrm{d}C_i(t)}{\mathrm{d}t} \propto F_i(t) \cdot \frac{1}{h(t)} \tag{1}$$

Applying Eq. (1) for both ^{222}Rn and CH_4, Equation (2) is obtained, with a dimensionless conversion factor c derived from the observed slope of the concurrent concentration increase in both gases:

$$\frac{\frac{\mathrm{d}C_{\mathrm{CH_4}}(t)}{\mathrm{d}t}}{\frac{\mathrm{d}C_{^{222}\mathrm{Rn}}(t)}{\mathrm{d}t}} \cdot F_{^{222}\mathrm{Rn}} = c \cdot F_{^{222}\mathrm{Rn}} = \mathrm{FR\_CH_4}, \tag{2}$$

observing the concentration increase in two gases that fulfil the above assumptions, here CH_4 and ^{222}Rn. If the flux of ^{222}Rn is known, then the flux of CH_4 can be calculated (Levin et al., 2011). A description of the specific criteria used to implement the RTM can be found in detail in Vogel et al. (2012). Grossi et al. (2014) previously applied the RTM for the first time at the GIC3 station using only a 3-month dataset and with a constant (in time and space) ^{222}Rn flux of 60 Bq m^{-2} h^{-1}. Here, in order to apply the RTM to retrieve

a time series of CH_4 fluxes (FR_CH_4) during 2013–2015 at the GIC3 station and to compare these results with those obtained using a bottom-up inventory for methane (FE_CH_4), we used the following extensive set-up:

1. A nocturnal window between 20:00 and 05:00 UTC was selected for each single night analysis in order to utilise only accumulation events in which atmospheric concentrations of both CH_4 and ^{222}Rn had a positive concentration gradient due to positive net fluxes under stable boundary layer conditions.

2. A data selection criterion based on a threshold of $R^2 \geq 0.8$ for the linear correlation between ^{222}Rn and CH_4 was used to reject events with low linear correlation between the atmospheric concentrations of both gases.

3. An *effective* radon flux influencing the GIC3 station each night from 2013 to 2015 was calculated by coupling local radon flux data, obtained using the output for the local pixel containing the GIC3 station of the model developed by López-Coto et al. (2013), with the footprints calculated by the ECMWF-FLEXPART model (version 9.02) (Stohl, 1998). Local radon flux data were calculated as explained in the following paragraph, while the footprints obtained are described in Sect. 2.4.3.

The radon flux model of the University of Huelva (from now on named the UHU model) employed in this work has been described in detail by López-Coto et al. (2013). By using this model, a time-dependent inventory was calculated for the period 2011–2014 by employing several dynamic inputs, namely soil moisture, soil temperature and snow cover thickness. These data were obtained directly from Weather Research and Forecasting (WRF) simulations (Skamarock et al., 2008). A domain of 97×97 grid cells centred on Spain with a spatial resolution of $27 \times 27\,km^2$ and a temporal resolution of 1 h was defined. The ^{222}Rn flux data calculated using this model were only available until November 2014 due to a lack of WRF simulations. In order to obtain data for this period when modelled ^{222}Rn flux data were not available, from December 2014 to December 2015, a seasonal and monthly climatology was calculated by using the UHU data set model for the years 2011–2014. Karstens et al. (2015) compared the ^{222}Rn flux values calculated over Europe by their model to UHU values and to long-term direct measurements of ^{222}Rn exhalation rates in different areas of Europe. They found a generally 40 % higher ^{222}Rn exhalation rate on their map than estimated by the UHU map over Europe. This previous result has been taken into consideration within the present study to better interpret the obtained data.

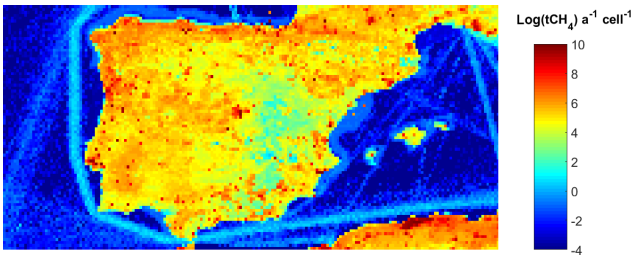

Figure 1. CH_4 EDGARv4.2 inventory grid map extracted for Spain (year 2010).

2.5 CH_4 fluxes based on FLEXPART footprints and the EDGARv4.2 inventory grid map

Bottom-up CH_4 fluxes influencing the GIC3 station were estimated by using the footprints calculated by the ECMWF-FLEXPART model (obtained as described in Sect. 2.4.3) and the Emissions Database for Global Atmospheric Research (EDGAR) version 4.2 (EDGAR, 2010). The EDGAR inventory, developed by the European Commission Joint Research Centre and the Netherlands Environmental Assessment Agency, includes global anthropogenic emissions of GHGs and air pollutants by country on a spatial grid. The EDGAR version used in the present study provides global annual CH_4 emissions on a 0.1° (11 km) resolution for the year 2010. All major anthropogenic source sectors, e.g. waste treatment, industrial and agricultural sources (e.g. enteric fermentation) are included, whereas natural sources (e.g. wetlands or rivers) are not. The spatial allocation of emissions on 0.1° by 0.1° grid cells in EDGAR has been built up by using spatial proxy datasets with the location of energy and manufacturing facilities, road networks, shipping routes, human and animal population density, and agricultural land use. UNFCCC reported national sector totals are then removed with the given percentages of the spatial proxies over the country's area (EDGAR, 2010). Figure 1 shows the EDGAR inventory grid map extracted for Spain.

The influence of the emissions associated with the cities surrounding the region of GIC3 was also modelled using this inventory to better understand their impact. In Table S1 the coordinates of the upper and lower corners of the areas used to describe the location of the metropolitan areas over the EDGAR inventory are reported.

2.6 Footprints

The Lagrangian particle dispersion model FLEXPARTv9.0.2 has been extensively validated and is nowadays widely used by the scientific community to calculate atmospheric source-receptor relationships for atmospheric gases and organic particles (e.g. Stohl, 1998; Stohl et al., 2005; Arnold et al., 2010; Font et al., 2013; Tohjima et al., 2014). FLEXPART allows computation of the trajectories of virtual air parcels arriving at the receptor point, i.e. the GIC3 station, at a specific

time. FLEXPART has been applied here to calculate 24 h backward trajectories of 10 000 virtual air parcels starting at 00:00 UTC for each night of the period 2013–2015. Each back trajectory simulation was run with a time-step output of 3 h. Meteorological data from the operational ECMWF-HRES model with a resolution of 0.2° were used as input fields for the FLEXPART modelling. The FLEXPART output domain resolution was 0.2°. The domain was set at 25° N, 40° W for the lowest left corner and 65° N, 10° W for the upper right corner. A nested output domain of 0.05° resolution was defined at 37° N, 12° W for the lowest left corner and 43° N, 0° E for the upper right corner. The FLEXPART model accounts for both the vertical and horizontal position of the virtual air parcels and their residence time in each grid cell. This information allows the influence of atmosphere–surface exchange to be estimated on the observed concentrations if air parcels are within the boundary layer. A maximum height of 300 m a.g.l. has been selected for the footprint analysis following Font et al. (2013). The average nocturnal footprint for the period 2013–2015 is presented in Fig. 2. The footprints obtained for the nested FLEXPART domain were combined with the EDGAR inventory map for CH_4 emissions (EDGAR, 2010) and with the UHU ^{222}Rn flux inventory map (López-Coto et al., 2013), separately, in order to obtain the time series of modelled CH_4 and *effective* ^{222}Rn fluxes. The resulting mean flux $F_i(S, t_n)$, for each gas i, at the receptor S (GIC3 station) and for each night t_n, with n ranging over the 3-year period, is thus given by Eq. (3):

$$F_i\,(\mathrm{S}, t_n) = \sum_{t=t_{no}}^{t=t_n} \sum_{x} F_i\,(\mathrm{x}, t_n) \cdot w\,(\mathrm{x}, \mathrm{T})\,, \qquad (3)$$

where t ranges between the 24 h of back-trajectories, $F_i(x, t)$ denotes the flux of a given grid cell x at time t derived from the EDGAR or UHU inventory map, separately. The weighting factor of each grid cell $w(x, T)$ is calculated using the FLEXPART footprint for each night t_n over the 3-year period and it has been calculated by normalising the residence time of each grid cell over the nested domain and during the 24 h back-trajectories (T), as given by Eq. (4):

$$\sum_{x,t}^{T} w(x, t) = 1. \qquad (4)$$

3 Results

In this section we present the results of the daily and seasonal atmospheric CH_4 variability at GIC3 station analysed using a record of 3-year hourly CH_4 and ^{222}Rn time series. Unfortunately, due to problems in the air sample system, data for 11 % of the time period are not available, mainly in the summer of 2013.

Grossi et al. (2016) presented a complete characterisation of the main meteorological conditions and ^{222}Rn behaviour

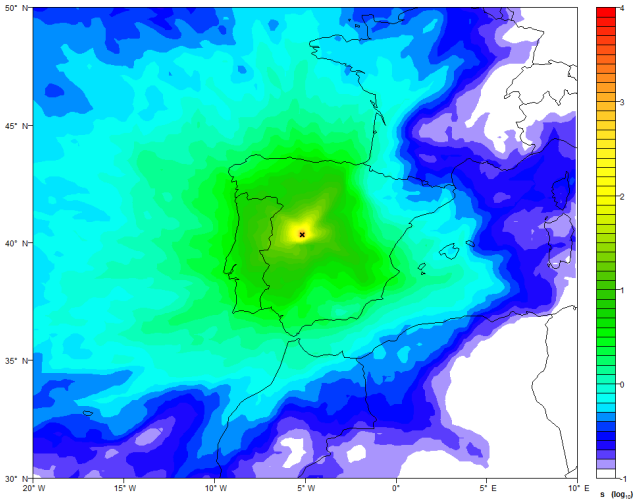

Figure 2. Average nocturnal FLEXPART footprint for the 2013–2015 period (residence time t is on the logarithmic scale).

at the ClimaDat stations including GIC3, and we will use these previous results to interpret atmospheric processes and the variability of CH_4 mixing ratio, as well as to understand the dominating wind regimes for CH_4 flux data analysis (Fig. S4 presents the monthly wind regimes observed at the GIC3 station both for day-time and night-time).

3.1 Statistics of the daily and seasonal atmospheric CH_4 variability

The 3-year hourly time series of atmospheric CH_4 mixing ratios measured at GIC3 shows a median value of 1904.5 nmol mol^{-1} with an absolute deviation of 29.6 nmol mol^{-1}. The box plots in Fig. 3 present the medians of the atmospheric CH_4 mixing ratios and ^{222}Rn concentrations measured at the GIC3 station over the dataset on an hourly (left panels) and a monthly (right panels) basis. Monthly means have been calculated separately for day-time (07:00–18:00 UTC) and night-time (19:00–06:00 UTC).

The maximum hourly median methane mixing ratio measured within the 3-year observation period is 1921.1 nmol mol^{-1} and is observed at 03:00 UTC, whereas the minimum hourly median value of 1889.9 nmol mol^{-1} is observed at 13:00 UTC. The absolute standard deviation of the hourly median is 16.97 nmol mol^{-1}. The hourly median daily amplitude at this station, between the minimum and the maximum, is 31.18 nmol mol^{-1}. CH_4 concentrations usually start decreasing at GIC3 in the morning at around 07:00 and 08:00 UTC and begin to increase again in the afternoon at around 17:00 and 18:00 UTC. Night-time CH_4 concentrations present an absolute standard deviation of 60 nmol mol^{-1}, while for day-time concentrations it is 30 nmol mol^{-1}. The same pattern is observed in the daily cycle of atmospheric ^{222}Rn (Grossi et al., 2016). Monthly day-time and night-time medians of CH_4 mixing ratios and ^{222}Rn

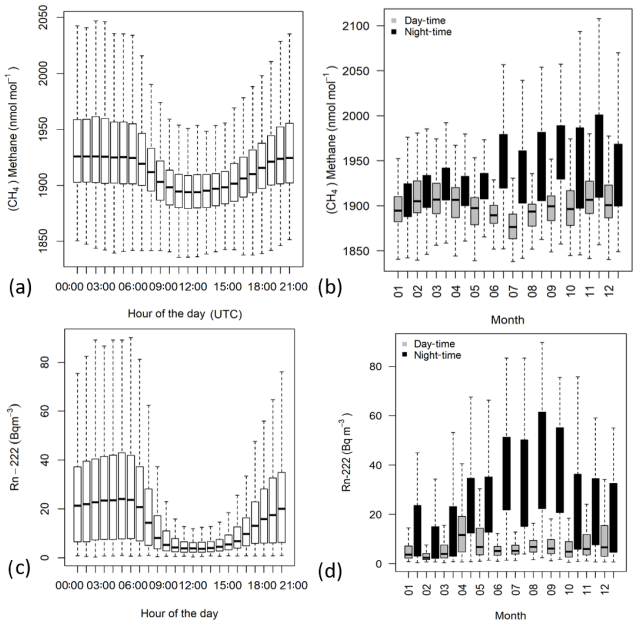

Figure 3. Box plots of hourly **(a, c)** and monthly **(b, d)** atmospheric CH_4 mixing ratios **(a, b)** and ^{222}Rn concentrations **(c, d)** measured from January 2013 to December 2015 at the GIC3 station. For each median (black bold line) the 25th (Q1; lower box limit) and 75th (Q3; upper box limit) percentiles are reported in the plot. The lower whisker goes from Q1 to the smallest non-outlier in the data set, and the upper whisker goes from Q3 to the largest non-outlier. Outliers are defined as > 1.5 IQR or < 1.5 IQR (IQR: interquartile range).

concentrations show different patterns, as seen in Fig. 3b, d. The night-time monthly medians of methane mixing ratio measured in the months between June and December look higher than those measured between January and May. Night-time monthly medians of measured ^{222}Rn concentration are highest between July and August.

3.2 Daily and seasonal PBLH variability

Figure 4 shows the hourly median (a) and the monthly median (b) variability of the PBLH data extracted from the ECMWF-HRES model for the grid containing the GIC3 station. On a daily basis the hourly median of the PBLH reaches its minimum during night-time between 23:00 and 07:00 UTC. The PBLH starts to increase at around 08:00 UTC, reaching its maximum between 14:00 and 16:00 UTC and then decreases again after 17:00 UTC. On a monthly basis, the day-time monthly median PBLH reaches its minimum during the winter months of January and December, while it reaches its maximum in the summer months. The highest night-time monthly medians for the PBL heights are observed in winter. The day-time monthly PBLH medians present a quite symmetric distribution (around July as a centre line), similar to the night-time monthly ^{222}Rn medians (Fig. 3d).

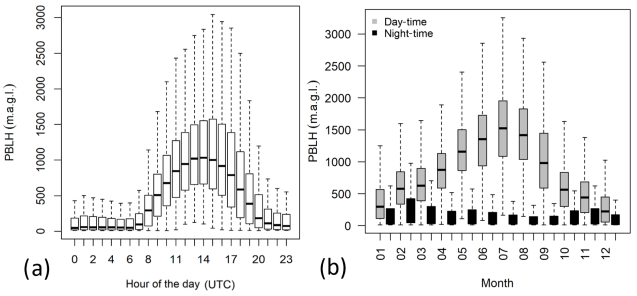

Figure 4. Box plots of hourly **(a)** and monthly **(b)** PBLH data extracted from the ECMWF-HRES model for the period January 2013–December 2015 at the GIC3 station. For each median (black bold line) the 25th (Q1; lower box limit) and 75th (Q3; upper box limit) percentiles are reported in the plot. The lower whisker goes from Q1 to the smallest non-outlier in the data set, and the upper whisker goes from Q3 to the largest non-outlier. Outliers are defined as > 1.5 IQR or < 1.5 IQR (IQR: interquartile range).

3.3 Comparison between CH_4 and ^{222}Rn variability

A comparison of the daily and seasonal variability of the atmospheric concentrations of ^{222}Rn and CH_4 in relation to changes in height of the PBL at the GIC3 station (2013–2015) is presented in Figs. 5 and 6, respectively.

The daily evolution of hourly means of the ^{222}Rn atmospheric concentrations (Fig. 5a) implies that on a daily timescale, when ^{222}Rn flux can be considered fairly constant (e.g. López-Coto et al., 2013), PBLH variations drive the increase or decrease in the atmospheric ^{222}Rn concentrations. In this sense, ^{222}Rn seems to be an excellent predictor of PBLH (and vice versa) on a daily timescale. Looking at the hourly means of the atmospheric CH_4 mixing ratios (Fig. 5b), we can observe that methane decreases as the PBLH increases, as was observed for ^{222}Rn. However, between 12:00 and 18:00 UTC higher values in CH_4 mixing ratios relative to the values observed between 10:00 and 12:00 UTC are observed, which have similar PBLH conditions and could indicate some daily variability in the methane fluxes.

To interpret the monthly variability, the daily amplitude for each gas, i.e. Δ^{222}Rn for radon and ΔCH_4 for methane, was calculated in order to subtract the influence of the changing daily background contribution measured at the GIC3 station. The term Δ^{222}Rn is defined as the difference between average night-time concentration data (19:00–06:00 UTC) versus average day-time (07:00–18:00 UTC) concentration data (Eq. 5), and ΔCH_4 has been calculated accordingly.

$$\Delta^{222}\mathrm{Rn}\left(=^{222}\mathrm{Rn}_{\mathrm{nighttime}}\right)-\left\langle^{222}\mathrm{Rn}_{\mathrm{day-time}}\right\rangle \quad (5)$$

Figure 6 reveals that monthly amplitudes increase in summer, when the day-time PBLH increases very strongly due to vertical mixing (see Fig. 4). This general tendency is found both for ^{222}Rn and CH_4 concentrations. Concentration am-

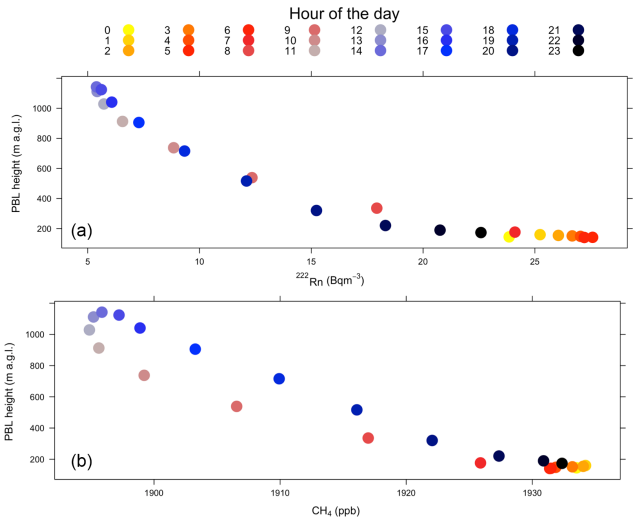

Figure 5. Relation between hourly means of atmospheric CH_4 **(b)** and ^{222}Rn **(a)** concentrations measured during 2013–2015 at the GIC3 station and ECMWF data of PBLH for the same area and for the same time interval.

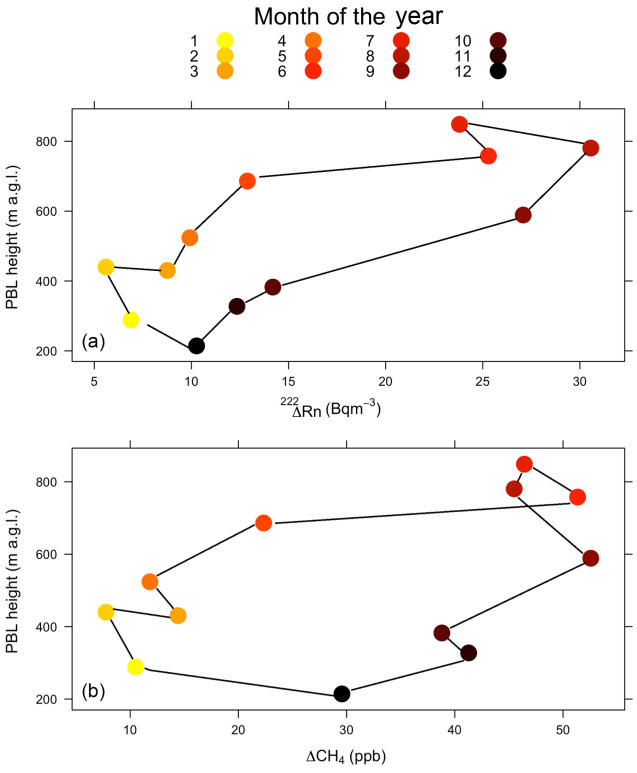

Figure 6. Relation between monthly means of concentration amplitudes of ΔCH_4 **(b)** and Δ^{222}Rn **(a)** measured during 2013–2015 at the GIC3 station and monthly ECMWF data of PBLH for the same area during same time interval.

plitudes of ^{222}Rn are higher in autumn than in winter under the same PBLH conditions (Fig. 6a). This could indicate that some process other than PBLH is driving this difference in the ^{222}Rn concentrations. In Fig. 7 we observe how the monthly ^{222}Rn flux calculated by the UHU model (presented in Sect. 2.4) changes.

In agreement with Grossi et al. (2016), we find a lower ^{222}Rn flux at GIC3 during winter due to snow cover events and low temperatures, which prevent ^{222}Rn diffusion from the soil. The ^{222}Rn flux then increases almost two-fold and three-fold during the autumn and summer months, respectively. This is due to drier soil conditions and the high gradient of temperature in the surface atmospheric layer which facilitates the escape of ^{222}Rn from the pores of the granitic soil (Nazaroff and Nero, 1988). This seasonality of the ^{222}Rn flux could be the main cause of the increased atmospheric Δ^{222}Rn under the same PBLH conditions.

Monthly variations of ΔCH_4 shown in Fig. 6 (bottom panel) display no clear simple correlation with PBLH. The ΔCH_4 appears to be higher between the months of June and December irrespective of the corresponding PBLH values.

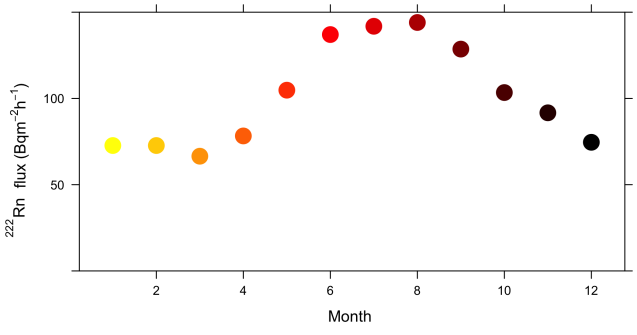

Figure 7. Monthly ^{222}Rn flux means calculated by the UHU model and climatology for 2013–2015 at the GIC3 station. Coloured circles indicate the same months as in Fig. 6.

3.4 Variations of CH_4 fluxes

So far, daily variations for both CH_4 mixing ratio and ^{222}Rn concentrations can be mainly explained in relation to the accumulation or dilution of gas concentrations within the PBL. However, the hysteresis observed for the CH_4 mixing ratio of Fig. 5b seems to indicate a small change in the methane source between 12:00 and 18:00 UTC.

Monthly Δ^{222}Rn variability can be understood when we account for seasonal ^{222}Rn flux changes. Unfortunately, existing emission inventories (EDGAR, 2010; MMA, 2016) generally do not yet provide seasonally, hourly varying CH_4 emission values either for Europe in general or for Spain in particular.

In order to understand the impact that temporal changes of CH_4 emissions may have on monthly mean atmospheric CH_4 mixing ratios, we have applied two different methodologies, as explained in Sect. 2.4.1 and 2.4.2, and we have compared their resulting fluxes: FR_CH_4 and FE_CH_4, respectively. Figure 8 presents the *effective* ^{222}Rn flux time series used

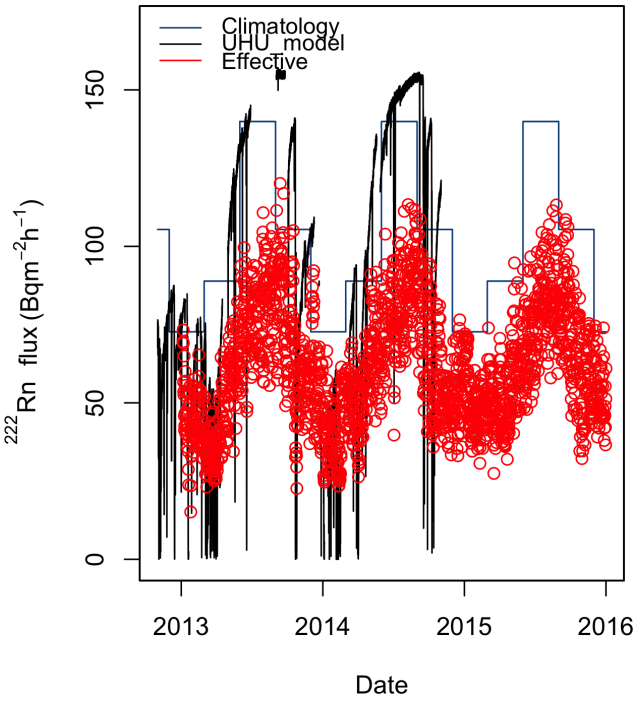

Figure 8. Time series of local ^{222}Rn flux calculated by the UHU model (black line; López-Coto et al., 2013) for the GIC3 area, ^{222}Rn flux seasonal climatology (blue line) and *effective* ^{222}Rn flux calculated on the basis of FLEXPART footprints (red dots). This last series was used within the RTM.

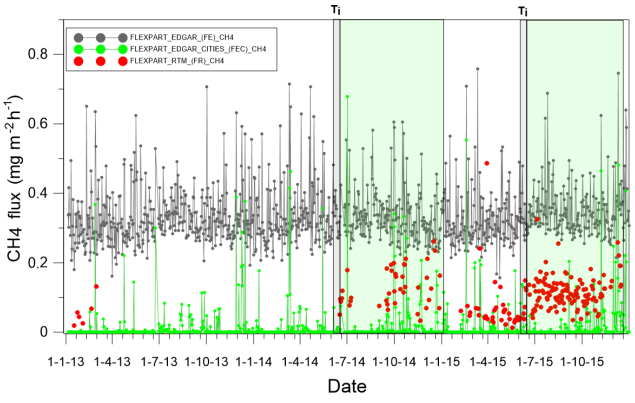

Figure 9. Results of night-time FR_CH_4 fluxes (mg CH_4 m^{-2} h^{-1}) (red circles) obtained at the GIC3 station from January 2013 to December 2015 compared with night-time FE_CH_4 fluxes obtained using bottom-up inventory emissions (grey line), and calculated FEC_CH_4 fluxes from contributions from surrounding cities (green circles). The weeks T_i represent the period of 2014 (21–27 June) and 2015 (20–26 June) when transhumant livestock returned to the GIC3 area after spending the winter in the south of Spain and concurrent with the availability of FR_CH_4 fluxes data. Shaded green regions represent the periods when transhumant livestock remain in the GIC3 area.

for the application of the first methodology (RTM), together with the raw ^{222}Rn flux calculated by the UHU model and its seasonal climatology.

Figure 9 presents the time series of CH_4 fluxes estimated at the GIC3 station and T_i (grey shaded rectangles) indicates the time when transhumant livestock returns to the GNP after spending the winter in the south of Spain (Tapias, 2014; Rodríguez, 2015). The green shaded areas indicate the periods, between June and December, when transhumant livestock typically stays in the GIC3 region (Ruiz Perez and Valero Sáez, 1990; López Sáez et al., 2009; Libro Blanco, 2013). Data coverage in the second part of the time series (2014–2015) is higher than in the first period (2013–2014) because the simultaneous availability of ^{222}Rn and CH_4 data was higher. The mean of FR_CH_4 fluxes over the dataset is 0.11 mg CH_4 m^{-2} h^{-1} with 25th and 75th percentiles of 0.07 and 0.14 mg CH_4 m^{-2} h^{-1}, respectively. The mean of FE_CH_4 fluxes over the dataset is 0.33 mg CH_4 m^{-2} h^{-1} with 25th and 75th percentiles of 0.28 mg CH_4 m^{-2} h^{-1} and 0.36 mg CH_4 m^{-2} h^{-1}, respectively. FR_CH_4 fluxes are constantly lower than FE_CH_4 fluxes, although this discrepancy decreases during some periods, as we will investigate later. FEC_CH_4 fluxes obtained with the EDGARv4.2 inventory by considering only the contribution of the cities that are located around the GIC3 station, in agreement with the masks presented in Table S1, had a total mean value over the dataset of 0.02 mg CH_4 m^{-2} h^{-1} with 25th and 75th percentiles of 0 mg CH_4 and 0.006 mg CH_4 m^{-2} h^{-1}, respectively.

Figure 10 shows monthly box plots of FE_CH_4 and FR_CH_4 fluxes. Shaded areas are coloured according to the main local wind directions reaching the GIC3 station at night. This classification is based on the results presented in Fig. S2, where monthly windrose plots for the GIC3 station between 2013 and 2015 are shown. We can observe that there is no variability in monthly FE_CH_4 flux values. In contrast, FR_CH_4 flux results show an increase in CH_4 fluxes between June and December that seems to be independent of the seasonally changing dominant wind directions. This increase is also uncorrelated with seasonally changing ^{222}Rn fluxes (Fig. 7). The seasonal change of CH_4 fluxes between the first and the second half of the year at GIC3 could indeed be related to variations in local CH_4 emissions. The period between June and December represents the time of year when transhumant livestock returns to the GNP.

The contribution of cities is only visible during certain months and it seems to be related with winds coming from the east in the direction of the Madrid urban area (see Fig. S2).

The disagreement observed between FE_CH_4 and FR_CH_4 fluxes in the months between June and December (Figs. 9 and 10), when the transhumant livestock is in the GIC3 area, may be due to different reasons:

1. A possible underestimation of the ^{222}Rn flux outputs from the UHU radon flux model could occur, which would lead to lower FR_CH_4 fluxes (Eq. 2). As ex-

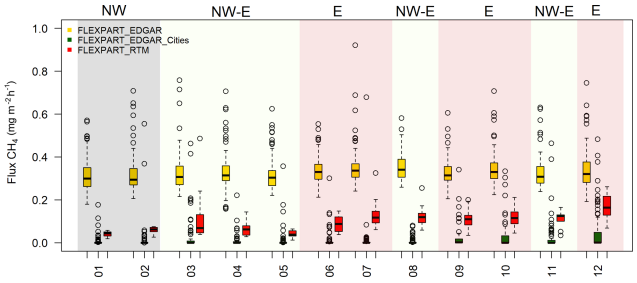

Figure 10. Box plots of monthly CH_4 fluxes (mg CH_4 m^{-2} h^{-1}) calculated for the GIC3 area using the RTM (red) and the EDGAR inventory (total in yellow; contribution of cities in green). Coloured areas indicate main wind directions for specific months. For each median (black bold line) the 25th (Q1; lower box limit) and 75th (Q3; upper box limit) percentiles are reported in the plot. The lower whisker goes from Q1 to the smallest non-outlier in the data set, and the upper whisker goes from Q3 to the largest non-outlier. Outliers are defined as > 1.5 IQR or < 1.5 IQR (IQR: interquartile range).

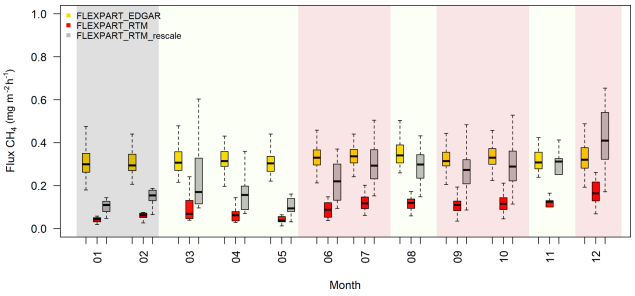

Figure 11. Box plots of monthly CH_4 fluxes (mg CH_4 m^{-2} h^{-1}) calculated for the GIC3 area using the RTM (red), the EDGAR inventory (yellow) and RTM using the ^{222}Rn flux comparison factor found by Karstens et al. (2015) (grey). Coloured areas indicate main wind directions for specific months. For each median (black bold line) the 25th (Q1; lower box limit) and 75th (Q3; upper box limit) percentiles are reported in the plot. The lower whisker goes from Q1 to the smallest non-outlier in the data set, and the upper whisker goes from Q3 to the largest non-outlier. Outliers are defined as > 1.5 IQR or < 1.5 IQR (IQR: interquartile range).

plained previously, Karstens et al. (2015) compared their radon flux model with the UHU model and it gave, generally, 40 % higher ^{222}Rn flux values than the UHU model over Europe.

2. The methodology used within the EDGAR for the spatial disaggregation of national sector emission over the country could lead to a distribution of CH_4 emission in the GIC3 region higher than true levels leading to an overestimation of the FE_CH_4.

3. The fixed height of 300 m used for the calculation of nocturnal footprints could introduce a bias. However, this value is well within the range of nocturnal PBLH values calculated with data extracted from the ECMWF-HRES model. Furthermore, the calculated FLEXPART footprints were used both for FR_CH_4 and FE_CH_4 calculations and this should not affect the relative differences between their values.

When applying a 40 % increase for the local ^{222}Rn source, as suggested by Karstens et al. (2015), we can re-calculate FR_CH_4 emissions as FR_CH_4_rescale. The box plot of the monthly medians of FE_CH_4, FR_CH_4 and FR_CH_4_rescale are compared in Fig. 11. The mean of FR_CH_4_rescale fluxes over the dataset is 0.29 mg CH_4 m^{-2} h^{-1} with 25th and 75th percentiles of 0.17 mg CH_4 and 0.34 mg CH_4 m^{-2} h^{-1}, respectively. FR_CH_4_rescale is in agreement with FE_CH_4 fluxes during the months between June and December, when the transhumant livestock remains in the GIC3 area (cattle season).

To highlight seasonal differences, FE_CH_4, FR_CH_4 and FR_CH_4_rescale fluxes are aggregated into two box plots in Fig. 12, according to the no-cattle season (January until May), when there is no livestock in the GIC3 area, and cattle season (June until December). According to these data during the no-cattle season, FR_CH_4 fluxes present a mean value of 0.09 CH_4 m^{-2} h^{-1} with a standard deviation of 0.15 mg CH_4 m^{-2} h^{-1}. During the cattle season, the mean value of FR_CH_4 fluxes is 0.12 CH_4 m^{-2} h^{-1} with a standard deviation of 0.05 mg CH_4 m^{-2} h^{-1}. The mean value of FR_CH_4_rescale fluxes is 0.24 mg CH_4 m^{-2} h^{-1} during the no-cattle season with a standard deviation of 0.39 mg CH_4 m^{-2} h^{-1} and it is 0.30 mg CH_4 m^{-2} h^{-1} during the cattle season with a standard deviation of 0.12 mg CH_4 m^{-2} h^{-1}. The corresponding values for FE_CH_4 fluxes are 0.31 mg CH_4 m^{-2} h^{-1} for the no-cattle season and 0.32 mg CH_4 m^{-2} h^{-1} for the cattle season.

4 Discussion

The present results show the different influences that meteorological conditions (PBLH and wind direction) and regional sources may have on the variability of atmospheric CH_4 concentrations observed at the GIC3 station. The ^{222}Rn observations have been used, together with modelled PBLH data, to better understand the reasons for the variability of the atmospheric CH_4 concentrations observed at the station for different times scales. The use of ^{222}Rn as a tracer to calculate independent fluxes of GHGs has been shown in order to help with the improvement of emission inventories on a regional scale.

4.1 Daily variability of atmospheric CH_4 concentrations

The daily cycle of atmospheric CH_4 mixing ratios (Fig. 3a) measured at GIC3 shows significant changes between daytime and night-time periods. The large increase in nocturnal CH_4 mixing ratios can mainly be explained by the decreased

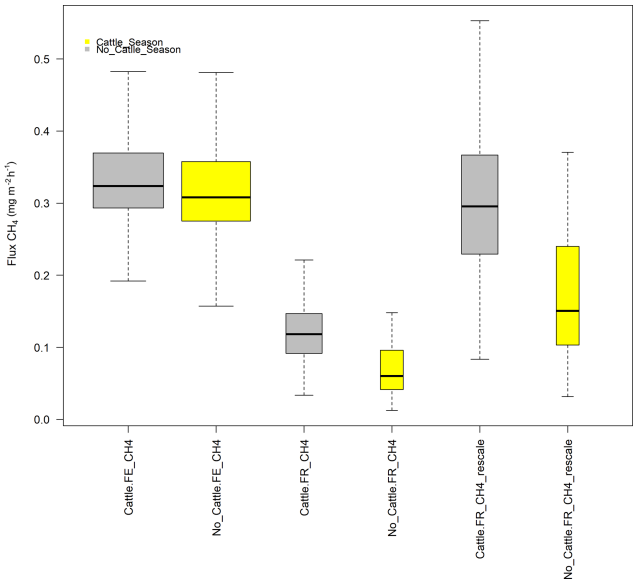

Figure 12. Box plots of FE_CH_4, FR_CH_4 and FR_CH_4_corr fluxes (in $mg\,m^{-2}\,h^{-1}$) calculated for theGIC3 area during the "warm" season (June–December, yellow box) and the "cold" season (January–May, grey box). For each median (black bold line) the 25th (Q1; lower box limit) and 75th (Q3; upper box limit) percentiles are reported in the plot. The lower whisker goes from Q1 to the smallest non-outlier in the data set, and the upper whisker goes from Q3 to the largest non-outlier. Outliers are defined as > 1.5 IQR or < 1.5 IQR (IQR: interquartile range).

height of the planetary boundary layer (Fig. 4a), which is supported by a similar behaviour of ^{222}Rn concentrations (Fig. 3c). Indeed, CH_4, as well as ^{222}Rn, reaches its maximum concentration when the PBLH is below 300 m a.g.l. during the night, while their atmospheric concentrations decrease with the increase in the PBLH during day-time.

The correlation of PBLH and ^{222}Rn (and CH_4) in Fig. 5 indicates that ^{222}Rn fluxes do not strongly vary on daily timescales or, at least, not to a degree that can influence their atmospheric concentration variability. CH_4 fluxes seem to change on a daily timescale. Average afternoon CH_4 concentrations are slightly enhanced compared to those from the morning for similar PBLH values (Fig. 5b). They show a hysteresis behaviour which could indicate local emissions increase or that a systematic transport of CH_4 enhanced air masses, not rich in radon, occurs at GIC3. Some studies (e.g. Bilek et al., 2001; Wang et al., 2015) have found strong emission increases from dairy cows after feeding in feedlots, while McGinn et al. (2010) only found small diurnal increases in CH_4 emissions between 11 and 17 h for grazing cattle. Unfortunately, no detailed information about the feeding cycle of the GIC3 livestock is available, but grazing should be considered the predominant form of livestock management in transhumance. However, Figs. 9 and 10 together with Fig. S4 show the influences of eastern winds, coming from the Madrid direction, on the CH_4 fluxes.

4.2 Seasonal variability of atmospheric CH_4 concentrations

To understand the drivers of monthly changing concentrations of CH_4, we need to account for PBLH local meteorology, changing regional emissions and changing background concentrations of CH_4 at GIC3. Median monthly mixing ratios for day-time and night-time (Fig. 3b) are discussed alongside ΔCH_4 (Fig. 6), which allows us to subtract seasonal and synoptic background variations. This enables us to focus on the impact of PBLH for individual days that are then averaged to investigate how ΔCH_4 changes on a monthly basis. The observed variability of ΔCH_4 (Figs. 3b and 6) cannot be explained only in terms of changes of the PBLH. Monthly averages of ΔCH_4 (and night-time monthly CH_4 box plots, Fig. 3b) present their maximum values between June and December, and their minimum values during the rest of the months irrespective of the height of the PBL. From co-located ^{222}Rn concentration observations we learn that an increase in the average monthly fluxes (Fig. 7) can compensate the effect of increased dilution in the deeper summer PBL on the observed concentrations (Fig. 6a), yielding similar atmospheric ^{222}Rn concentrations. The increase in the modelled ^{222}Rn flux in the GIC3 region from the winter to autumn season and the following decrease can coherently help to explain the variation observed in monthly Δ^{222}Rn. Thus, the comparison between ΔCH_4 and Δ^{222}Rn suggests that there may also be a monthly variability in the sources of CH_4 which should help to understand monthly atmospheric mixing ratios variability. This has been further confirmed by our FR_CH_4 flux estimates, as seen in Figs. 9, 10 and 11. Of course, the FR_CH_4 flux estimates are limited to night-time due to the RTM hypothesis. FR_CH_4 fluxes show a total mean value 33 % lower than FE_CH_4 fluxes over the data set. When ^{222}Rn fluxes are rescaled according to Karstens et al. (2015), this difference is drastically reduced to 10–15 %.

RTM-based CH_4 fluxes show an increase of 25 % during the second semester of the year on a monthly basis. This increase coincides with the period of the year when transhumant livestock resides in the GIC3 region. Although no exact information is available on the number of animals present only in the GIC3 area, during this period of enhanced ruminant emissions, the difference between CH_4 fluxes based on RTM and the EDGAR inventory is reduced from 73 to 65 % for FR_CH_4 and from 27 to 9 % for FR_CH_4_rescale The difference during the no-cattle season is likely due to the constant annual emission factor of CH_4 emission used within the bottom-up inventory which, of course, cannot yet reflect transhumance activity. The likely explanation is that all emissions from the aforementioned animals has been constantly allocated to this region, which is why FE_CH_4 is also larger than FR_CH_4_rescale during months when they are

not present. The RTM analysis performed here suggests that transhumance could be a relevant process to the understanding of sub-annual CH_4 emissions in the region and can affect the spatial distribution of CH_4 sources within a country. Our study indicates that the choice of ^{222}Rn model has an important impact on annual total emissions calculated, while seasonal and short-term patterns are preserved.

5 Conclusions and outlook

To gain a full picture of the Spanish (and European) GHG balance, understanding of CH_4 emissions in different regions is a critical challenge, as is the improvement of bottom-up inventories for all European regions. Our study uses, among other elements, GHG, meteorological and ^{222}Rn tracer data from one of the eight stations of the new ClimaDat network in Spain, which provides continuous atmospheric observations of CH_4 and ^{222}Rn in a region of Europe. The present study underlines the fact that this data, combined with retrieved PBLH data and atmospheric transport modelling (FLEXPARTv92) can help to understand the main causes of temporal variability of GHG mixing ratios and can offer new insights into regional emissions by identifying the impacts of changing sources, e.g. emissions from transient livestock.

These first promising results should lead to further application of this RTM to other GHG time series from the ClimaDat network and potentially in continent-wide networks such as ICOS that routinely perform co-located GHG and ^{222}Rn observations. Particularly, the usefulness of the RTM has been shown, while also highlighting the need to improve this method, especially in regard to (i) validation of the ^{222}Rn flux maps applied within the RTM and (ii) standardization of the footprint calculation.

Although the transhumant livestock seems to be the likely reason for the seasonal changes observed in the FR_CH_4 fluxes at the GIC3 station, other sources could also contribute to this seasonality, such as waterbodies or other natural emissions. These previous sources are not included in the EDGAR inventory, but they could be detected by the RTM. However, those sources would not be able to fully explain the sudden onset of increased RTM-based CH_4 fluxes but would rather contribute to a slow increase in warmer months. Further research applying isotopic analysis of CH_4 mixing ratios measured at the GIC3 station for the different seasons should be carried out, as well as transects of the regions to assess the impact of natural sources on CH_4 mixing ratios. In addition, no precise data on transhumant activity in Spain is available to date, but our study suggests the existence of a link between regional CH_4 fluxes and highlights the need for more information on transhumance activity which could be taken into account in future emission inventories of this region (and Europe). In addition, our results show that urban emissions can be transported and could influence the atmospheric composition of remote rural areas over several hundred kilometres under specific synoptic conditions.

Data availability. The datasets are available at http://www.climadat.es/es/datos/.

The Supplement related to this article is available online at https://doi.org/10.5194/acp-18-5847-2018-supplement.

Competing interests. The authors declare that they have no conflict of interest.

Acknowledgements. The research leading to these results has received funding from "la Caixa" Foundation with the ClimaDat project (2010–2014) and from the Ministerio Español de Economía y Competividad, Retos 2013 (2014–2016) with the MIP (Methane interchange between soil and air over the Iberian Península) project (reference: CGL2013-46186-R). This study was also made possible thank to collaboration with the Autonomous Community of Castile and León and the Sierra de Gredos Regional Park.

Claudia Grossi particularly thanks the Ministerio Español de Educación, Cultura y Deporte, for partially supporting her work with the research mobility grant "José Castillejos" (ref. CAs15/00042). The research of Felix R. Vogel has been funded and supported by the Chaire industrielle BridGES, a joint research program between ThalesAleniaSpace, Veolia and the parent institutions of LSCE (CEA, CNRS, UVSQ).

The authors warmly thank (i) the LAO (Atmosphere and Ocean laboratory) team, in the persons of Rosa Arias, Manel Nofuentes, Oscar Batet, Lidia Cañas, Silvia Borras, Paola Occhipinti and Eusebi Vazquez, for their efforts in the installation, maintenance and calibration of all IC3 climatic stations and data, including the GIC3 station, where this study has been performed; (ii) the INTE team, in the persons of Vicente Blasco and Juan Antonio Romero, for their work in the building of the ARMON installed at the GIC3 station; (iii) Albert Jornet, software engineer of the IC3, who developed, together with Roger Curcoll, an automatic system for the daily running of FLEXPART backward simulations; (iv) Israel Lopéz-Coto and the University of Huelva for the radon flux modelled data; (v) Stefano Galmarini for helping to improve the paper; (vi) David Carslaw and Karl Ropkins, developers of the R package OpenAir (www.openair-project.org, last access: February 2015), used in the present work for data analysis; and (vi) the two anonymous reviewers for their comments and suggestions for improving our work.

Edited by: Paul O. Wennberg
Reviewed by: two anonymous referees

References

Àgueda, A., Grossi, C., Pastor, E., Rioja, E., Sánchez-García, L., Batet, O., Curcoll, R., Ealo, M., Nofuentes, M., Occhip-

inti, P., Rodó, X., and Morguí, J.-A: Temporal and spatial variability of ground level atmospheric methane concentrations in the Ebro River Delta, Atmos. Pollut. Res., in press, https://doi.org/10.1016/j.apr.2017.01.009, 2018.

Arnold, D., Vargas, A., Vermeulen, A., T., Verheggen, B., and Seibert, P.: Analysis of radon origin by backward atmospheric transport modelling, Atmos. Environ., 44, 494–502, https://doi.org/10.1016/j.atmosenv.2009.11.003, 2010.

Bergamaschi, P., Krol, M., Meirink, J. F., Dentener,F., Segers, A., van Aardenne, J., Monni, S., Vermeulen, A. T., Schmidt, M., Ramonet, M., Yver, C., Meinhardt, F., Nisbet, E. G., Fisher, R. E., O'Doherty, S., and Dlugokencky, E. J.: Inverse modelling of European CH_4 emissions 2001–2006, J. Geophys. Res., 115, D22309, https://doi.org/10.1029/2010JD014180, 2010.

Crosson, E. R.: A cavity ring-down analyzer for measuring atmospheric levels of methane, Carbon dioxide and water vapor, Appl. Phys. B, 92, 403–408, https://doi.org/10.1007/s00340-008-3135-y, 2008.

De Ramus, H. A., Clement, T. C., Giampola, D. D., and Dickison, P. C.: Methane Emissions of Beef Cattle on Forages: Efficiency of Grazing Management Systems, J. Environ. Qual., 32, 269–277, https://doi.org/10.2134/jeq2003.2690, 2003.

EDGAR: Emission Data Base for Global Atmospheric Research release version 4.1 of the European Commission, Joint Research Center (JRC)/Netherland Environmental Assessment Agency (PBL), available at: http://edgar.jrc.ec.europa.eu/index.php# (last access: April 2018), 2010.

EEA: European Environment Agency CORINE Land Cover. Corine Land Cover technical guide, available at: http://www.eea.europa.eu/publications/tech40add (last access: May 2016), 2007.

European Center for Medium-Range Weather Forecasting: Diagnostic boundary layer height, in IFS Documentation CY31r1, vol. 4, Physical Processes, Reading, UK, available at: http://www.ecmwf.int/sites/default/files/elibrary/2007/9221-part-iv-physical-processes.pdf (last access: February 2015), 2006.

FAO: The State of Food Insecurity in the World 2013. The multiple dimensions of food security, Rome, FAO, available at: http://www.fao.org/docrep/018/i3434e/i3434e.pdf (last access: January 2015), 2013.

Font, A., Grimmond, C. S. B., Morguí, J.-A., Kotthaus, S., Priestman, M., and Barratt, B.: Cross-validation of inferred daytime airborne CO_2 urban-regional scale surface fluxes with eddy-covariance observations and emissions inventories in Greater London, Atmos. Chem. Phys. Discuss., 13, 13465–13493, https://doi.org/10.5194/acpd-13-13465-2013, 2013.

Griffiths, A. D., Parkes, S. D., Chambers, S. D., McCabe, M. F., and Williams, A. G.: Improved mixing height monitoring through a combination of lidar and radon measurements, Atmos. Meas. Tech., 6, 207–218, https://doi.org/10.5194/amtd-5-6835-2012, 2012.

Grossi, C., Arnold, D., Adame, J. A., López-Coto, I., Bolívar, J. P., de la Morena, B. A., and Vargas, A.: Atmospheric ^{222}Rn concentration and source term at El Arenosillo 100 m meteorological tower in southwest Spain, Radiat. Meas., 47, 149–162, https://doi.org/10.1016/j.radmeas.2011.11.006, 2012.

Grossi, C., Vogel, F. R., Morguí, J. A., Curcoll, R., Àgueda, A., Batet, O., Nofuentes, M., Occhipinti, P., Vargas, A., and Rodó, X.: First estimation of CH_4 fluxes using the ^{222}Rn tracer method over the central Iberian Peninsula, in Air Pollution XXII, WIT Trans. Ecol. Environ., 183, 233–245, https://doi.org/10.2495/AIR140201, 2014.

Grossi, C., Àgueda, A., Vogel, F. R., Vargas, A., Zimnoch, M., Wach, P., Martín, J. E., López-Coto, I., Bolívar, J. P., Morguí, J.-A., and Rodó, X.: Analysis of ground-based ^{222}Rn measurements over Spain: filling the gap in southwestern Europe, J. Geophys. Res.-Atmos., 121, 11021–11037, https://doi.org/10.1002/2016JD025196, 2016.

Hammer, S. and Levin, I.: Seasonal variation of the molecular hydrogen uptake by soils inferred from continuous atmospheric observations in Heidelberg, southwest Germany, Tellus B, 61, 556–565, https://doi.org/10.1111/j.1600-0889.2009.00417.x, 2009.

Hernández, M. A.: Ávila concentra el 85 % de la ganadería trashumante que pervive en España, available at: www.cadenaser.com/emisora/2016/04/18/ser_avila/1460979067_721996.html, last access: May 2016.

Hiller, R. V., Bretscher, D., DelSontro, T., Diem, T., Eugster, W., Henneberger, R., Hobi, S., Hodson, E., Imer, D., Kreuzer, M., Künzle, T., Merbold, L., Niklaus, P. A., Rihm, B., Schellenberger, A., Schroth, M. H., Schubert, C. J., Siegrist, H., Stieger, J., Buchmann, N., and Brunner, D.: Anthropogenic and natural methane fluxes in Switzerland synthesized within a spatially-explicit inventory, Biogeosciences, 11, 1941–1959, https://doi.org/10.5194/bg-11-1941-2014, 2014.

IPCC: Intergovernmental Panel on Climate Change, Climate Change 2013: the physical science basis, in: Contribution of working group I to the fifth assessment report of the Intergovernmental Panel on Climate Change, edited by: Stocker, T. F., Qin, D., Plattner, G. K., Tgnor, M., Alle, S., Boshung, J., Nauels, A., Yu Xia, Bex, V., and Midgley, P., available at: https://www.ipcc.ch/pdf/assessment-report/ar5/wg1/WG1AR5_Frontmatter_FINAL.pdf (last access: April 2018), 2013.

Jeong, S., Ying-Kuang, H., Andrews, A. E., Bianco, L., Vaca, P., Wilezak, J. M., and Fischer, M. L.: A multitower measurement network estimate of California's methane emissions, J. Geophys. Res.-Atmos., 118, 1–13, https://doi.org/10.1002/jgrd.50854, 2013.

Levin, I., Hammer, S., Eichelmann, E., and Vogel, F. R.: Verification of greenhouse gas emission reductions: the prospect of atmospheric monitoring in the polluted areas, Philos. T. Roy. Soc. A, 369, 1906–1924, https://doi.org/10.1098/rsta.2010.0249, 2011.

Libro Blanco: La trashumancia en España. Red rural nacional, Secretaría General de Agricultura y Alimentación. Dirección General de Desarrollo Rural y Política Forestal, Subdirección General de Modernización de las Explotaciones, available at: www.magrama.gob.es/es/desarrollo-rural/publicaciones/publicaciones-de-desarrollo-rural/LIBRO_BLANCO_2013_tcm7-245950.pdf (last access: May 2016), 2013.

López-Coto, I., Mas, J. L., and Bolívar, J. P.: A 40-year retrospective European radon flux inventory including climatological variability, Atmos. Environ., 73, 22–33, https://doi.org/10.1016/j.atmosenv.2013.02.043, 2013.

López Sáez, J. A., López Merino, L., Sánchez, F. A., and Pérez Díaz, S.: Contribución paleoambiental al studio de la trashumancia en el sector abulense de la Sierra de Gredos, Hispania LXIX, 231, 9–38, ISSN: 0018-2141, 2009.

MMA: Ministerio de Medio Ambiente, Inventario de emisiones de gases de efecto invernadero de España. Años 1990–2014, Comunicación al secretariado de la convención marco de NNUU sobre cambio climático, Secretaría General para la Prevención de la Contaminación y del Cambio Climático, Dirección General de Calidad y Evaluación Ambiental, Subdirección General de Calidad del Aire y Prevención de Riesgos, Madrid, 1–1212, available at: www.magrama.gob.es/es/calidad-y-evaluacion-ambiental/temas/sistema-espanol-de-inventario-sei-/nir_ed2016_def_tcm7-417776.pdf (last access: May 2016), 2016.

Nazaroff, W. W. and Nero, A. V. (Eds.): Radon and its decay products in indoor air, John Wiley & Sons, New York, USA, 57–106, https://doi.org/10.1063/1.2810982, 1988.

NRC: Committee on Methods for estimating Greenhouse Gas Emissions of the National Research Council: Verifying greenhouse gas emissions, Washington (DC), The National Academic Press, 2010.

Prinn, R. G.: Measurement equation for trace chemicals in fluids and solution of its inverse, Geophys. Monogr. Ser., 114, 3–8, https://doi.org/10.1029/gm114p0003, 2000.

Rella, C.: Accurate Greenhouse Gas Measurements in Humid Gas Streams Using the Picarro G1301 Carbon Dioxide/Methane/Water Vapor Gas Analyzer, White Paper, Picarro Inc., Sunnyvale, CA, USA, 2010.

Rodríguez, M.: Más de 400 reses trashumantes regresan a Gredos, Diario de Avila, available at: www.diariodeavila.es/noticia/ZB81ABF36-CC0C-2ABE-4545305C6871EB6E/20150621/mas/400/reses/trashumantes/regresan/gredos, last access: 20 June 2015.

Ruiz Perez, M. and Valero Sáez, A.: Transhumance with cows as a rational land use option in the Gredos Mountains (Central Spain), Human Ecol., 18, 187–202, https://doi.org/10.1007/bf00889182, 1990.

Schery, S. D. and Wasiolek, M. A.: Modeling Radon Flux from the Earth surface, in Radon and Thoron in the human environment, World Scientific Pubblishing, 207–217, https://doi.org/10.2172/607500, 1998.

Schmidt, M., Graul, R., Sartorius, H., and Levin, I.: Carbon dioxide and methane in continental Europe: a climatology, and ^{222}Radon-based emission estimates, Tellus B, 48, 457–473, 1996.

Schmithüsen, D., Chambers, S., Fischer, B., Gilge, S., Hatakka, J., Kazan, V., Neubert, R., Paatero, J., Ramonet, M., Schlosser, C., Schmid, S., Vermeulen, A., and Levin, I.: A European-wide ^{222}radon and ^{222}radon progeny comparison study, Atmos. Meas. Tech., 10, 1299–1312, https://doi.org/10.5194/amt-10-1299-2017, 2017.

Seidel, D., Zhang, Y., Beljaars, A., Golaz, J.-C. Jacobson, A., and Medeiros, B.: Climatology of the planetary boundary layer over the continental United States and Europe, J. Geophys. Res., 117, D17106, https://doi.org/10.1029/2012JD018143, 2012.

Skamarock, W. C., Klemp, J. B., Dudhia, J., Gill, D. O., Barker, D. M., Duda, M. G., Huang, X.-Y., Wang, W., and Powers, J. G.: A Description of the Advanced Research WRF Version 3, NCAR Technical Note, NCAR/TN–475+STR, 2008.

Stohl, A., Hittenberger, M., and Wotawa, G.: Validation of the Lagrangian particle dispersion model FLEXPART against large scale tracer experiments, Atmos. Environ., 32, 4245–4264, https://doi.org/10.1016/s1352-2310(98)00184-8, 1998.

Szegvary, T., Conen, F., and Ciais, P.: European ^{222}Rn inventory for applied atmospheric studies, Atmos. Environ., 43, 1536–1539, https://doi.org/10.1016/j.atmosenv.2008.11.025, 2009.

Tapias, R. M.: De Mombeltrán al puerto del Pico, con la vaca avileña, El Mundo, Madrid, available at: www.elmundo.es/madrid/2014/07/01/53b1a5d3e2704e99368b4585.html, last access: 1 July 2014.

Tohjima, Y., Kubo, M., Minejima, C., Mukai, H., Tanimoto, H., Ganshin, A., Maksyutov, H., Katsumata, K., Machida, T., and Kita, K.: Temporal changes in the emissions of CH_4 and CO from China estimated from CH_4 / CO_2 and CO / $COCO_2$ correlations observed at Hateruma Island. Atmos. Chem. Phys., 14, 1663–1677, https://doi.org/10.5194/acp-14-1663-2014, 2014.

Troen, I. and Mahrt, L.: A simple model of the atmospheric boundary layer: Sensitivity to surface evaporation, Bound.-Lay. Meteorol., 37, 129–148, https://doi.org/10.1007/BF00122760, 1986.

Van der Laan, S., Karstens, U., Neubert, R. E. M., Van der Laan-Luijkx, I. T., and Meijer, H. A. J.: Observation-based estimates of fossil fuel-derived CO_2 emissions in the Netherlands using Δ^{14}C, CO and ^{222}Radon, Tellus B, 62, 389–402, https://doi.org/10.1111/j.1600-0889.2010.00493.x, 2010.

Vargas, A., Arnold, D., Adame, J. A., Grossi, C., Hernández-Ceballos, M. A., and Bolívar, J. P.: Analysis of the vertical radon structure at the Spanish "El Arenosillo" tower station, J. Environ. Radioact., 139, 1–17, https://doi.org/10.1016/j.jenvrad.2014.09.018, 2015.

Vermeulen, A. T., Pieterse, G., Hensen, A., Van den Bulk, W. C. M., and Erisman, J. W: COMET: a Lagrangian transport model for greenhouse gas emission estimation – forward model technique and performance for methane, Atmos. Chem. Phys. Discuss., 6, 8727–8779, https://doi.org/10.5194/acpd-6-8727-2006, 2006.

Vogel, F. R., Ishizawa, M., Chan, E., Chan, D., Hammer, S., Levin, I., and Worthy, D. E. J.: Regional non-CO_2 greenhouse gas fluxes inferred from atmospheric measurements in Ontario, Canada, J. Integr. Environ. Sci., 9, 1–15, https://doi.org/10.1080/1943815X.2012.691884, 2012.

Wada, A., Matsueda, H., Murayama, S., Taguchi, S., Hirao, S., Yamazawa, H., Moriizumi, J., Tsuboi, K., Niwa, Y., and Sawa, Y.: Quantification of emission estimates of CO_2, CH_4 and CO for East Asia derived from atmospheric radon-222 measurements over the western North Pacific, Tellus B, 65, 18037, https://doi.org/10.3402/tellusb.v65i0.18037, 2013.

WWF: International World Wide Fund For Nature: Editor Barney Jeffries, Spanish version by Mar Rego, ISBN 978-2-940443-84-0, 2014.

Zahorowski, W., Chambers, S. D. A., and Henderson-Sellers, A.: Ground based radon-222 observations and their application to atmospheric studies, J. Environ. Radioact., 76, 3–33, https://doi.org/10.1016/j.jenvrad.2004.03.033, 2004.

Zimnoch, M., Wach, P., Chmura, L., Gorczyca, Z., Rozanski, K., Godlowska, J., Mazur, J., Kozak, K., and Jericevic, A.: Factors controlling temporal variability of near-ground atmospheric ^{222}Rn concentration over central Europe, Atmos. Chem. Phys. 14, 9567–9581, https://doi.org/10.5194/acp-14-9567-2014, 2014.